BEST AVAILABLE IMAGES

Defective images within this document are accurate representations of the original documents submitted by the applicant.

Defects in the images may include (but are not limited to):

- BLACK BORDERS
- TEXT CUT OFF AT TOP, BOTTOM OR SIDES
- FADED TEXT
- ILLEGIBLE TEXT
- SKEWED/SLANTED IMAGES
- COLORED PHOTOS
- BLACK OR VERY BLACK AND WHITE DARK PHOTOS
- GRAY SCALE DOCUMENTS

IMAGES ARE BEST AVAILABLE COPY.

As rescanning documents *will not* correct images, please do not report the images to the Image Problem Mailbox.

ELSEVIER

Sensors and Actuators A 55 (1996) 65–69

SENSORS AND ACTUATORS A PHYSICAL

Process for in-plane and out-of-plane single-crystal-silicon thermal microactuators

J. Mark Noworolski [a], Erno H. Klaassen [b], John R. Logan [c], Kurt E. Petersen [c], Nadim I. Maluf [b,c,*]

[a] *Department of Electrical Engineering, 207-194, Cory Hall, U.C. Berkeley, Berkeley, CA 94720, USA*
[b] *Center for Integrated Systems, CIS 130, Stanford University, Stanford, CA 94305-4070, USA*
[c] *Lucas NovaSensor, 1055 Mission Court, Fremont, CA 94539, USA*

Abstract

A process to manufacture single-crystal thermal actuators using silicon fusion bonding and electrochemical etch stop is presented. The process permits the simultaneous creation of in-plane and out-of-plane thermal actuators together with levers suitable for both directions of actuation. A final dry-release step is used, permitting the manufacture of MOS or bipolar devices in conjunction with actuators. Out-of-plane actuation of vertically levered devices has been demonstrated. The −3 dB response frequency of out-of-plane actuators is approximately 1000 Hz in air. Novel levered in-plane devices which achieve deflections of up to 200 μm have been fabricated. An estimate of the upper bound of thermal actuator efficiency is presented.

Keywords: Single-crystal-silicon thermal actuators; In-plane thermal actuators; Out-of-plane thermal actuators; Silicon levers; Thermal actuator efficiency; CMOS compatible; Aluminum–silicon bimorph

1. Introduction

Actuation on the microscale is of interest for a variety of applications, such as r.f. and optical switching, fluid and gas manipulation, and for the handling of small objects. Several actuation mechanisms have been demonstrated for microactuators. Electrostatic forces have found uses in comb-drive elements for in-plane motion [1], as well as deformable mirror devices for out-of-plane motion [2]. Magnetic forces, generally provided by an off-chip source, have also been demonstrated for both in-plane and out-of-plane deflection [3]. Thermal expansion effects utilizing either monomorph [4] or bimorph structures [5,6] have also been demonstrated. Other thermal actuators include plated-nickel structures employing differential heating effects [7,8].

This paper presents a variety of in-plane and out-of-plane thermal actuators fabricated in single-crystal silicon using a single process flow. Thermal expansion effects operate over only relatively short distances, but are capable of producing very large forces. For example, a singly supported 100 μm long silicon beam, which undergoes a uniform temperature increase ΔT of 100°C, will expand only 26 nm. At the same time, however, the beam is capable of exerting a force of 49 μN per square micrometer of cross-sectional area. By comparison, for an electrostatic actuator with an inter-plate spacing of 2 μm and a drive voltage of 10 V, the force developed is 0.1 μN per square micrometer of capacitive area.

In order to provide useful actuation, it is often necessary to provide a mechanism to trade force for operating distance. In this paper, we present a process that permits the fabrication of thermal-motion amplification schemes in both in-plane and out-of-plane directions, and offer several examples of these.

2. Fabrication process

The single-crystal-silicon microactuators presented here are fabricated by using silicon fusion bonding, electrochemical etchback [9,10], and dry etching [12]. A simplified process flow is shown in Fig. 1.

In the first step, a 10 μm cavity is anisotropically etched into a p-type handle wafer (Fig. 1(a)). Simultaneously, an alignment mark is placed on the back of the wafer to facilitate double-sided alignment of patterns to the cavity during later processing steps. Next, a p-type wafer with an n-type epitaxial layer is fusion bonded to the cavity side of the handle wafer (Fig. 1(b)). The thickness of the epitaxial layer determines

* Corresponding author. Lucas NovaSensor. Tel: (510) 661 6000. Fax: (510) 770 0645.

PII S0924-4247(96)01251-4

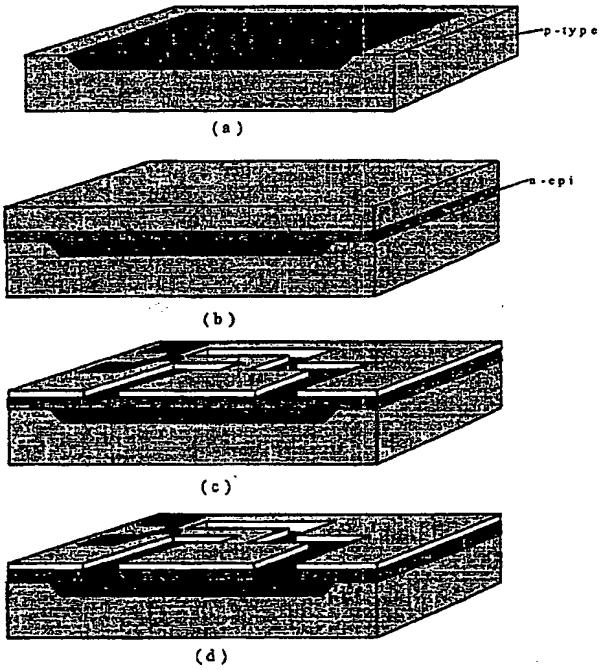

Fig. 1. Simplified process flow for the fabrication of the thermal actuators. (a) A cavity is etched in a p-type handle wafer. (b) A p-type wafer with an n-type epitaxial layer is fusion bonded to the cavity side of the handle wafer. An electrochemical etch stop is then used to etch away the exposed p-type on top of the structure, leaving only the n-epitaxial layer attached to the handle wafer. (c) Implant and metallization steps are performed, and the wafer is patterned with the actuator patterns. (d) A plasma etch through the n-epitaxial diaphragm into the underlying cavity releases the structures.

the height of the finished thermal actuators. Epitaxial layer thicknesses used in this process ranged from 3 to 28 μm. Following the silicon fusion bond anneal, the exposed p-substrate of the epitaxial layer is etched away. An electrochemical etch stop [11] is used to stop the etch accurately on the n-epilayer during this step.

Further processing then provides p-type diffused resistors and metallization, which are indirectly aligned to the buried cavity by using the alignment marks on the backside of the handle wafer. At this point additional processing may be performed to integrate any desired circuitry on the top wafer surface. The wafer is then patterned (Fig. 1(c)), and the structures released using a dry etch (Fig. 1(d)). The final dry-etch release facilitates the use of aluminum as a metallization layer, thereby also permitting the creation of bimorph force-actuated thermal devices.

A simplified process flow using a heavily doped (0.05 Ω cm) p-type bonded-on wafer and a deep reactive ion etching release step [12] was used to prepare additional wafers with up to 50 μm device thickness. For these wafers, the device thickness was controlled by a grind and polish step instead of an electrochemical etch stop. Note that the heavily doped starting material is an adequate conductor, thus the metallization and implantation steps were omitted from the process flow shown in Fig. 1.

The process presented allows the fabrication of in-plane as well as out-of-plane thermal actuators by tailoring the thickness of the epitaxial layer. In general, for in-plane actuation, a thicker n-epilayer is used, while for out-of-plane thermal actuation, a thin silicon layer is fabricated. If both in-plane and out-of-plane actuators are desired on the same wafer, an intermediate epitaxial layer thickness can provide adequate performance for both actuation methods.

3. Results and discussion

Wafers using the above process were fabricated with epitaxial layer thicknesses of 3 and 28 μm. The thick wafers were used for tests of in-plane devices, while the thin epitaxial layer wafers were used for out-of-plane device tests. All wafers were processed with identical masks including lateral as well as out-of-plane thermal actuator structures.

3.1. In-plane devices

Fig. 2 shows a scanning electron micrograph (SEM) of a device that operates in the lateral direction when current is passed through it. The device contains one contiguous implanted resistor. The resistance of the narrower part of the device is higher than that of the wide side. When a current is passed through the heating resistor, more power dissipates in the narrow leg, causing it to expand more than the wider side. This differential thermal expansion can be compared with that of a bimorph structure. Since the two sides are attached with cross-members, the difference in expansion causes the device to move laterally, in the plane of the chip. Devices with a 28 μm thick epitaxial layer achieved lateral deflections of 5 μm with an input power of 160 mW in air.

Fig. 3 shows a thermal actuator that operates on a different principle. In this device current is passed through the long, slightly angled beams. As they expand they press against the center bridging beam, thus causing a deflection of the center pointer device. This device amplifies the motion of the expanding beams following the expression $\delta y = \cot(\theta)\,\delta x$, where δy is the motion of the central beam, θ is the interior angle of the heater beams ($\approx 170°$), and δx is the expansion of the heaters. With a 28 μm thick and 8 μm wide device,

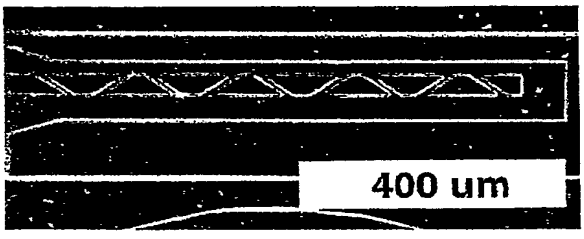

Fig. 2. A scanning electron micrograph of a lateral thermal actuator.

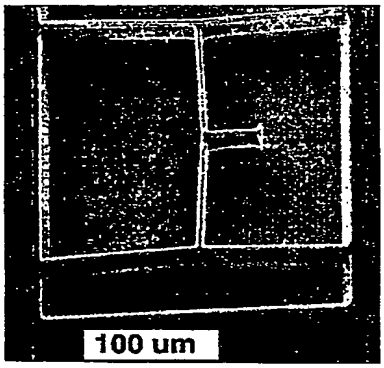

Fig. 3. A scanning electron micrograph of a lateral parallel-type thermal actuator structure.

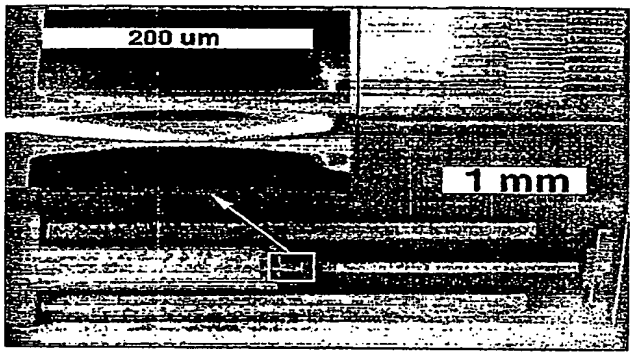

Fig. 4. A scanning electron micrograph of a differentially driven levered thermal actuator.

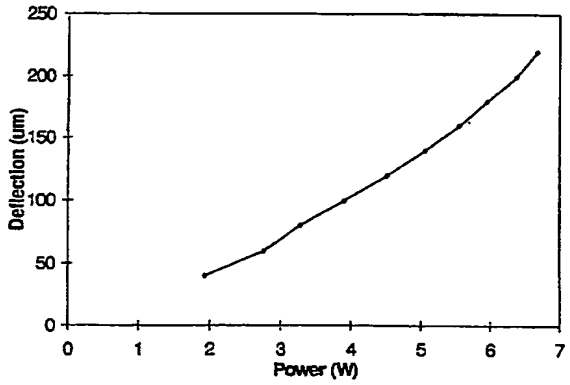

Fig. 5. Deflection of the actuator shown in Fig. 4 as a function of input power.

deflections as large as 10 μm have been observed with 280 mW of input power in air.

An example of a lever system to amplify motion in the in-plane direction is shown in Fig. 4. In the plane of the SEM, current through the heaters causes expansion in the horizontal direction; the lever system then magnifies this displacement to produce a vertical deflection of the pointer. This device, 50 μm thick, produces a deflection proportional to the difference in mean-square currents through the two drive branches. The results of a single-sided excitation at varying power levels are shown in Fig. 5.

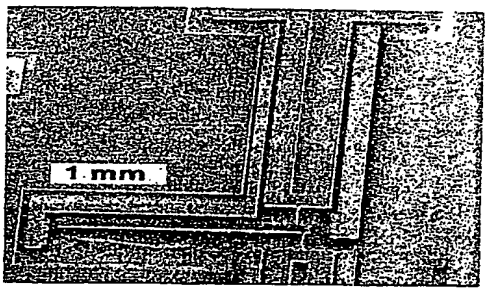

Fig. 6. A scanning electron micrograph of an in-plane thermal device with deflection amplification.

Another in-plane levered device, shown in Fig. 6, utilizes a lever system to provide additional gain for a given power level. Two U-shaped heaters expand when electrical power is dissipated in them. They then push inward, from opposite sides, somewhat offset from a common point, against a silicon beam. Deflections of the top and bottom drive elements are amplified by the pointer assembly. With only one electrode driven, deflections of 100 μm have been observed at an input power of 5.5 W.

3.2. Out-of-plane devices

Out-of-plane thermally actuated levered devices (Fig. 7, Fig. 8) can also be fabricated using this process. By patterning two cavities on either side of a thin sliver of silicon during the initial etch of the handle water, a thin slightly recessed fulcrum can be created. In this case, the following silicon fusion bonding step does not result in the formation of a bond at that junction. The right side of the device shown in Fig. 7 is a heater resistor covered with a layer of aluminum, thus creating a bimorph force into the plane of the page. This force causes the large area to bend down until it hits the lever beam, at which point a mechanical advantage is obtained in deflection.

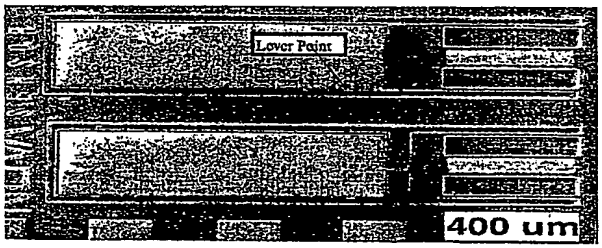

Fig. 7. A scanning electron micrograph of a vertically levered out-of-plane thermal actuator.

Fig. 8. A cross-sectional view of a vertical lever.

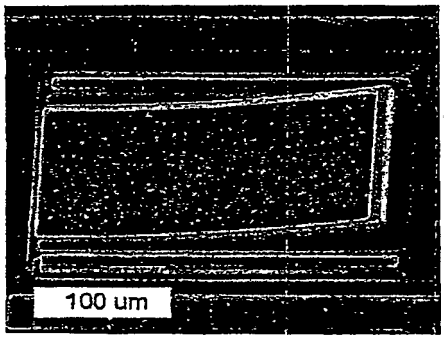

Fig. 9. A scanning electron micrograph of a single vertically deflecting thermal actuator.

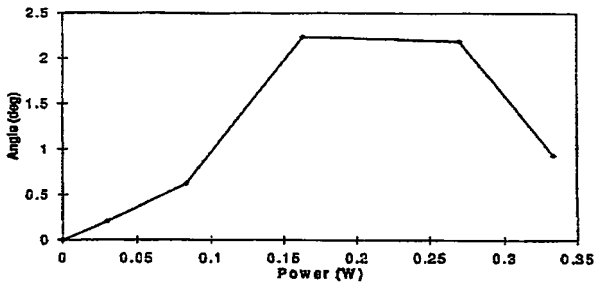

Fig. 10. Steady state deflection of vertical thermally actuated mirror array element shown in Fig. 9 as a function of input power.

A different type of vertically deflecting device, not requiring a fulcrum, uses the buckling of a thermally heated beam against a semi-rigid point. Fig. 9 shows part of a 10×10 matrix addressable array of vertically deflecting thermally actuated mirrors operating using this principle. The picture shown corresponds to an undriven case; the exhibited flexing is due to a residual stress in the surface aluminum layer. Current is passed through one side beam, through the thin supporting region and out the other long side beam. Most of the thermal expansion is realized in the side beams, exerting a force on the support beam to effect a torque, thereby resulting in a large deflection of the large center area. In Fig. 9, the aluminum covering the large center area causes a bimorph actuation into the plane of the photograph due to the heating of the center area. A measurement of the response of the device to an a.c. low voltage waveform superimposed on a d.c. bias shows a −3 dB bandwidth of 1000 Hz in air.

The same device was also subjected to varying d.c. loads under atmospheric ambient conditions. As can be seen in Fig. 10, the deflection is limited to approximately 2° at 18 mW. This limitation is reached when the tip of the device flexes enough to reach the bottom of the cavity. Any further increase in power bends the main reflective area, thereby decreasing the angle seen. The deflection of the device was also observed in a vacuum under different power levels via a feedthrough mechanism in an SEM. Due to the lack of convective losses, increased deflections were observed for a given power level at reduced pressures.

4. Conclusions

We have demonstrated a process suitable for the manufacture of thermal actuators. The process is compatible with both in-plane and out-of-plane thermal actuators, as well as MOS and bipolar circuits. Results have been presented demonstrating a 2° deflection with a power input of 18 mW for out-of-plane devices with a 3 dB bandwidth of approximately 1000 Hz. In-plane devices have shown deflections of up to 200 μm.

The manufactured devices are made of stress-free single-crystal silicon, permitting large geometries to be patterned. The use of aluminum as a metallization material also permits the creation of bimorph actuated devices.

A derivation of the upper bound on efficiency for a single-beam thermal actuator has been presented (see Appendix). Thermal heating was shown to produce large forces but with a low efficiency as compared to electrostatic actuation.

Acknowledgements

The authors would like to thank Rose Scimeca without whose dedication to detail this process would not be complete. We are also greatly indebted to Ken Honer of Stanford University for assistance in the use of the laser measurement system. We would also like to thank Alcatel Comptech for performing the final release etch on the 28 μm thick wafers, and STS for the final release of the 50 μm thick wafers. This work was sponsored by ARPA contract DAAL 01-94-C-3411.

Appendix A

In order to obtain an upper bound on efficiency for a thermally actuated structure, we consider a simple one-dimensional geometry and neglect losses due to convection and radiation. The actuation mechanism is assumed to be thermal expansion due to a step input of current of duration t seconds through a singly supported beam of length L with a constant temperature at the support end ($x=L$).

When driven in vacuum, it has been shown that the temperature distribution within the beam is [13]

$$T(x,u) = \frac{A_0 L^2}{2K} \times \left\{ 1 - \frac{x^2}{L^2} - \frac{32}{\pi^3} \sum_{n=0}^{\infty} \frac{(-1)^n}{(2n+1)^3} \cos\left[\frac{(2n+1)x\pi}{2L}\right] \times \exp\left[\frac{-u(2n+1)^2\pi^2}{4}\right] \right\} = \frac{A_0 L^2}{2K} t(x,u) \quad (1)$$

where A_0 is the heat generation per unit volume within the beam, L is the length of the beam, K is the thermal conductivity of the material, u is the dimensionless quantity $Kt/cL^2\rho$, c is the heat capacity, t is the time during which a heating current is passed through the beam, and ρ is the density of the material. By integration of the thermal expansion equation with the calculated temperature distribution, an expression for the net deflection, $dl(u)$ of the beam is obtained:

$$dl(u) = \frac{\alpha A_0 L^2}{2K}\left\{\frac{2}{3} - \frac{64}{\pi^4}\sum_{n=0}^{\infty}\frac{1}{(2n+1)^4} \times \exp\left[\frac{-u(2n+1)^2\pi^2}{4}\right]\right\} = \frac{\alpha A_0 L^2}{2K} l(u)$$

where α is the coefficient of thermal expansion.

Noting that the energy stored in a beam which expands by dl is

$$E_{out} = \frac{1}{2}\frac{EA}{L}dl^2$$

and that the total energy supplied to the system is $E_{in} = A_0 LAt$, we form an expression for the efficiency:

$$\eta = \frac{E_{out}}{E_{in}} = \frac{1}{2}\frac{E}{A_0 L^2 t}dl^2 = \frac{1}{4}\frac{E\alpha^2}{Kc\rho}A_0\frac{l(u)^2}{u} \quad (2)$$

where E is the Young's modulus of the material, and A is the cross-sectional area.

In conjunction with appropriate constraints, Eqs. (1) and (2) can be used to optimize thermal actuator geometry and performance.

Capacitively driven structures, once actuated, require no additional energy to maintain their position. In contrast, thermal actuators require a supply of power to maintain an actuated position.

Eq. (2) shows that work is done most efficiently in thermal actuators when they are driven by short-duration high-power pulses.

References

[1] W.C. Tang, T.-C.H. Nguyen, M.W. Judy and R.T. Howe, Electrostatic-comb drive of lateral polysilicon resonators, *Sensors and Actuators, A21–A23* (1990) 328–331.

[2] L.J. Hornbeck, Deformable-mirror spatial light modulators, *SPIE Proc.*, Vol. 1150, 1990, pp. 86–102.

[3] J.W. Judy and R.S. Muller, Magnetic microactuation of torsional polysilicon structures, *Sensors and Actuators A, 52–54* (1996) 392–397.

[4] J.W. Judy, T. Tamagawa and D.L. Polla, Surface micromachined linear thermal microactuator, *Tech Digest, IEEE Int. Electron Devices Meet., New York, USA, 1990*, pp. 629–632.

[5] M. Ataka, A. Omodaka, N. Takeshina and H. Fujita, Fabrication and operation of polyimide bimorph actuators for a ciliary motion system, *J. Microelectromech. Syst.*, 2 (1993) 146–150.

[6] J.W. Suh, C.W. Storment and G.T.A. Kovacs, Characterization of multi-segment organic thermal actuators, *Tech. Digest, 8th Int. Conf. Solid-State Sensors and Actuators (Transducers '95)/Eurosensors IX, Stockholm, 25–29 June, 1995*, pp. 333–335.

[7] H. Guckel, J. Klein, T. Christenson, K. Skrobis, M. Laudon and E.G. Lovell, Thermo-magnetic metal flexure actuators, *IEEE Solid State Sensors Workshop, Hilton Head, SC, USA, 1992*, pp. 73–77.

[8] L.A. Field, D.L. Burriesci, P.R. Robrish and R.C. Ruby, Micromachined 1×2 optical fiber switch, *Sensors and Actuators A, 52–54* (1996) 311–315.

[9] K.E. Petersen, D. Gee, F. Pourahmadi, R. Craddock, J. Brown and L. Christel, Surface micromachined structures fabricated with silicon fusion bonding, *Proc. 6th Int. Conf. Solid-State Sensors and Actuators (Transducers '91), San Francisco, CA, USA, 24–28 June, 1991*, pp. 397–399.

[10] C.H. Hsu and M.A. Schmidt, Micromachined structures fabricated using a wafer bonded sealed cavity process, *Tech. Digest, IEEE Solid State Sensors Workshop, Hilton Head, SC, USA, 1994*, pp. 151–155.

[11] B. Kloeck, S.D. Collins, N.F. de Rooij, R.L. Smith, Study of electrochemical etch-stop for high precision thickness control of silicon membranes, *IEEE Trans. Electron Devices, 36* (1989) 663–669.

[12] E.H. Klaassen, K. Petersen, J.M. Noworolski, J. Logan, N.I. Maluf, J. Brown, C. Storment, W. McCulley and G.T.A. Kovacs, Silicon fusion bonding and deep reactive ion etching; a new technology for microstructures, *Tech. Digest, 8th Int. Conf. Solid-State Sensors and Actuators (Transducers '95)/Eurosensors IX, Stockholm, 25–29 June, 1995*, pp. 556–559.

[13] H.S. Carslaw and J.C. Jaeger, *Conduction of Heat in Solids*, Oxford University Press, London, 2nd edn., 1959.